ORIGINAL ARTICLE

Synthesis and characterization of nanocomposites containing *Buchholzia coriacea* pod decorated with multi-walled carbon nanotubes for remediation of rhodamine B dye from aqueous solution

James Friday Amaku[1] · Raymond Taziwa[1]

Abstract

A novel nanocomposite (WKM) was synthesized by crosslinking *Buchholzia coriacea* pod (WK) and *f*-MWCNTs for the efficient adsorption of rhodamine B (RhB) from wastewater. The uptake of RhB onto WK and WKM was influenced by initial pH, adsorbent dose, the temperature of the adsorptive system, contact time and initial RhB concentration. Optimum experimental conditions of 100 min agitation time, 0.05 g dosage, solution pH 3.0 and 100 mg dm^{-3} initial concentration were obtained. The uptake of RhB onto WK and WKM was well expressed by Freundlich isotherm and a monolayer maximum uptake capacity of 67.82 mg g^{-1} and 87.58 mg g^{-1} was determined for WK and WKM, respectively. The adsorption of RhB onto WKM and WK followed the Elovich and pseudo-first-order kinetic models, respectively. Thermodynamic parameters such as $\Delta G°$, $\Delta H°$ and $\Delta S°$ reveal that the uptake of RhB onto WK and WKM was spontaneous and endothermic. Meanwhile, WKM demonstrated excellent reusability. Hence, this study presents a nanocomposite (WKM) with robust potential for RhB removal.

Keywords Adsorption · Thermodynamics · Nanocomposite · MWCNTs · *Buchholzia coriacea*

Introduction

Colour-imparting chemicals are widely employed in numerous industries such as pharmaceuticals, cosmetics, textiles, plastic, printing and food. These chemicals are also used in biotechnology as a staining fluorescent (Jain et al. 2007). Hence, a large amount of untreated wastewater containing toxic dyes is produced across the globe (Sarwar and Khan 2022). The indiscriminate discharge of industrial effluents containing dyes can cause devastating environmental pollution (Ukaogo et al. 2020). Among these colour-imparting chemicals is rhodamine B (RhB). RhB is a basic cationic dye that belongs to the xanthene class (Wu and Gao 2009). It is also one of the most extensively used water-soluble dyes in various industries.

RhB has an intravenous median lethal (LD$_{50}$) of 89.5 mg kg^{-1}; hence, it tends to be harmful if consumed beyond the threshold concentration (Mittal and Mishra 2014). RhB can cause irritation to the eyes, skin and respiratory tract if a small amount is swallowed by man. On the other hand, high exposure to this RhB may cause neurotoxicity, adverse reproductive and developmental effects, and cancer (Marking 1969; Skjolding et al. 2021). Photosynthetic activity in the aquatic ecosystem is hindered due to the high tinctorial value of RhB. The complexity of RhB molecules confers great stability on it against biodegradation, oxidizing agents and photo-degradation. This makes it difficult to eliminate from the aquatic ecosystem.

To avert the health implication of RhB on both man and aquatic organisms. Stakeholders have intensified their effort towards the design of a robust and effective technique for the elimination of RhB from wastewater. Several physicochemical techniques have been assessed and reported for the sequestration of RhB from the aquatic ecosystem and they include adsorption (Hayeeye et al. 2017; Wang et al. 2017; Zamouche and Hamdaoui 2012), electrochemical oxidation

✉ James Friday Amaku
famaku@wsu.ac.za

Raymond Taziwa
rtaziwa@wsu.ac.za

1   Department of Applied Science, Faculty of Science Engineering and Technology, Walter Sisulu University, Old King William Town Road, Potsdam Site, East London 5200, South Africa

(Du et al. 2012), chemical oxidation (Chang et al. 2009b), electro-oxidation and photocatalysis (Zhao and Zhu 2006) and photocatalytic oxidation (Jain et al. 2007). A comparison of the aforementioned techniques presented adsorption as an alternative method for the adsorption of RhB from aqueous solution and this could be due to its user-friendliness, rapidness, low cost and superior efficiency. Meanwhile, the effectiveness of different adsorbents to eliminate RhB from wastewater has been investigated and these adsorbents include activated carbon (Kadirvelu et al. 2005), CNT (Kumar et al. 2014), fly ash (Gupta et al. 2000), cedar con (Zamouche and Hamdaoui 2012), Fe_3O_4 magnetic nanoparticles (Mittal and Mishra 2014), montmorillonite (Selvam et al. 2008), bentonite (Hou et al. 2011) kaolinite (Khan et al. 2012) and biomass (Das et al. 2006),

Recently, nano-scaled materials have gained the attention of experts and stakeholders in water remediation practices. The ability of nanomaterials to sequester dyes from wastewater is generally attributed to their large surface area, high number of adsorption sites and reduced diffusion resistance (Liu et al. 2013; Vyawahare et al. 2014). Nanomaterials such as multi-walled carbon nanotubes (MWCNTs) demonstrated superior capacity for the adsorptive removal of both organic and organic and inorganic pollutants from industrial effluent (Abdullah et al. 2022; Adewoye et al. 2021; Lim et al. 2023). This excellent uptake capacity MWCNTs could be attributed to their superior physicochemical properties (Vinod Kumar Gupta et al. 2013; Vinod K Gupta and Saleh 2013). *Buchholzia coriacea* is commonly called wonderful kola and is mostly cultivated in Africa. Previous reports showed that this plant has great medicinal value, but its pod is often discarded as waste. The pod as biomass can be converted into useful material if modified and applied as adsorbents for wastewater remediation. Previous study showed that the combination of biomass and MWCNTs birth nanocomposites with superior capacity for environmental remediation practice (Hoang et al. 2022; Khalatbary et al. 2022). In this research, a novel nanocomposite (WKM) was fabricated from *Buchholzia coriacea* pod (WK) and *f*-MWCNTs. The applicability of WKM and WK in RhB adsorption was assessed in view of operational adsorptive variables, kinetics models, isotherms models and thermodynamics.

Materials and methods

Rhodamine B powder (98.98%), sulphuric acid (H_2SO_4) (98%), multi-walled carbon nanotubes (95%), triethylenetetramine (99.99%), nitric acid (HNO_3) (99.9%), sodium hydroxide (NaOH) (99.98%), sodium chloride (NaCl) ($> 95\%$) and hydrochloric acid (HCl) (99.9%) were purchased from Sigma-Aldrich.

Samples and sample preparation

Buchholzia coriacea were purchase from Orieugba market (5° 53′ 71″ North, 7. 7° 49′ 97″ East) in Umuahia Abia state, Nigeria. The plant was declared not endangered. Thereafter, the pod was washed using deionized water, oven-dried at 80 °C and pulverized to a fine powder using an electric grinder and stored in an airtight container.

Functionalization of MWCNTs

About 0.5 g of MWCNTs was immersed in 25 cm^3 of 6 M HCl at room temperature for 1 h on stirring and thereafter diluted 10 times using deionized water and then filtered under vacuum. The product obtained was subsequently treated with 6 M NHO_3 using a similar procedure. The purified MWCNTs (*p*-MWCNTs). 0.25 g of *p*-MWCNTs was immersed in a concentrated (HNO_3:H_2SO_4) 100 cm^3 of a mixture of acid (1:3 by volume) at room temperature. The mixture was stirred for 12 h and afterwards diluted 20 times its initial volume using deionized water and then filtered under vacuum. The product obtained was washed under a vacuum until the pH of the water was obtained. The black product (*f*-MWCNTs) obtained was vacuum-dried (80 °C) for 24 h and thereafter stored in an airtight container for future application.

Preparation of nanocomposite

About 0.5 g of *f*-MWCNTs and 2 g of WK were weighed into a beaker containing 50 cm^3 of deionized water, the mixture was stirred at room temperature for 3 h. Subsequently, triethylenetetramine (1 cm^3) was added to the mixture (*f*-MWCNTs/WK). At 90 °C, the mixture was then agitated to dryness, vacuum oven-dried, designated as WKM and stored in an airtight container for further use.

Characterization

The specific surface area of WKM and WK was investigated using the BET analysers (Micromeritics Instruments Corp., USA). WKM and WK were characterized using the Fourier-transformation infrared spectroscopy (FTIR) (Termo Nicolet-870 spectrophotometer, USA). The field-emission scanning electron microscope (ZEISS ultra plus, USA) was used to characterize the surface morphology of the adsorbents. The thermal behaviour of the nanocomposite was examined using the PerkinElmer simultaneous thermal analyser (STA6000 instrument, USA).

pH point of zero charges (pH$_{PZC}$)

To determine the pH$_{PZC}$ of WKM and WK, by using the solid addition method (Balistrieri and Murray 1981; Belachew and Hinsene 2020; Zubrik et al. 2017). Eleven Erlenmeyer flasks containing 50 cm^3 of 0.1 mol dm^{-3} NaCl solution adjusted to the pH range of 2–12 were contacted with 0.1 g of WKM or WK. The mixtures were stoppered and agitated for 48 h at room temperature. The pH$_{PZC}$ of WKM and WK were evaluated from the plot of the final pH versus the initial pH of the mixture.

Batch adsorption

The removal of RhB by WKM and WK was achieved using the batch adsorption technique. About 25 cm^3 (100 mg dm^{-3}) of RhB was contacted with WKM or WK in a 100 cm^3 stoppered glass bottle for 180 min. The mixture was equilibrated using a pre-set thermostatic water bath shaker at room temperature for 180 min and filtered using filter paper (Whatman No 1). The effect of pH (solution pH varied from 1 to 10 (using 0.1 M HCl and 0.01 M NaOH) with mass; 0.05 g, time: 180 min and concentration: 100 mg dm^{-3}), contact time (time was varied from 5 to 180 min with mass; 0.05 g, pH: 3 and concentration: 100 mg dm^{-3}), adsorbent dose (dosage was varied from 0.01 to 1 g with solution pH: 3, time: 180 min and concentration: 100 mg dm^{-3}) and initial concentration (initial RhB concentration was varied from 10 to 100 mg dm^{-3} with mass; 0.05 g, pH: 3 and contact time: 180 min) were examined. The implication of solution temperature was also assessed within the temperature range of 298–318 K. The experiments were performed in duplicates. The equilibrium concentration of RhB was estimated by making use of a UV–Visible spectrophotometer at 554 nm. The uptake potential and the % adsorption of WKM and WK were calculated using the equation displayed in the supplementary information (see Eq S1 & S2).

Isotherm and kinetics and models

The kinetics responsible for the adsorption of RhB onto WKM and WK were assessed by making use of the pseudo-first-order, pseudo-second-order, intraparticle diffusion and Elovich kinetics models as displayed in Table 1. On the other hand, the experimental data obtained from initial RhB concentration experiment over a known temperature range (298–313 K) were fixed into two isotherm models which include Freundlich and Langmuir (see Table 2).

Regeneration study

Reusability of the spent WKM and WK was achieved via the adsorption–desorption technique. The aforementioned adsorption procedure was used to load RhB onto WKM and WK and thereafter desorbed using aqueous ethanol. About 0.05 g of the spent adsorbent (WKM–RhB or WK–RhB) was contacted with 10 cm^3 of absolute ethanol in a 100 cm^3 stoppered glass bottle for 20 min at room temperature. The regenerated WKM and WK were cleaned with deionized water and dried in preparation for the next cycle. The percentage uptake of WKM and WK for the next cycle was calculated using Eq. S2 (see supplementary information).

Table 2 Isotherm models used to describe the uptake of RhB onto WKM and WK

Isotherm model	Equation	Parameters	References
Langmuir	$q_e = \frac{q_{max}bC_e}{1+bC_e}$	q_{max}, b	Langmuir (1918)
Freundlich	$q_e = K_F C_e^{1/n}$	k_F, n	HMF Freundlich (1906)

q_{eq}, adsorption capacity (mg g^{-1}); C_{eq}, equilibrium concentration of adsorbate in solution (mg dm^{-3}); q_{max}, maximum monolayer capacity (mg g^{-1}); b, Langmuir isotherm constant (dm^3 mg^{-1}); K_F, Freundlich isotherm constant (mg g^{-1}) (dm^{-3} mg^{-1})^n; n, adsorption intensity

Table 1 Kinetics models investigated for the adsorption of RhB onto WKM and WK

Kinetic models	Equations	Parameters	References
Pseudo-first order	$\frac{dq_t}{d_t} = k_1(q_e - q_t)$	q_e, k_1	Aksu and Karabayır (2008)
Pseudo-second order	$\frac{dq_t}{d_t} = k_2(q_e - q_t)^2$	k_2, q_e	Sevim et al. (2011)
Weber–Morris intraparticle diffusion	$\frac{dq_t}{d_{r-0.5}} = k_{id}$	k_{id}, l	Ofomaja et al. (2009)
Elovich	$\frac{dq_t}{d_t} = \alpha \exp(-\beta q_t)$	α, β	Omorogie et al. (2016)

k_1, pseudo-first-order rate constant (min^{-1}); k_2, pseudo-second-order rate constant (g mg^{-1} min^{-1}). k_{id}, intraparticle diffusion rate constant (mg g^{-1} min$^{0.5}$); l, is a constant related to the boundary layer thickness (mg g^{-1}); q_t, quantity of adsorbate adsorbed at time t (mg g^{-1}); q_e, quantity of adsorbate adsorbed at equilibrium (mg g^{-1}); α, adsorption rate constant (mg g^{-1} min^{-1}); β, desorption rate constant (g mg^{-1})

Results and discussion

The microstructure and surface morphology of the as-prepared and RhB-loaded adsorbent was assessed using FESEM analysis. The FESEM micrograph of the pristine biomass (WK) was noticed to have an agglomerate of irregular-shaped mass with apertures of varied diameter. Meanwhile, the RhB-loaded WK was noticed to have a smooth surface sustaining irregular sheets (see Fig. 1). On the other hand, the nanocomposite was observed to exhibit a lump-like shape that is clustered with a filament-like long rod having uniform diameters. This shows a successful fabrication of the nanocomposite, it also reflects the homogeneity of WKM. The nanocomposite exhibited swelling characteristics after the adsorption of RhB molecules. This shows that RhB molecules were adsorbed onto the surface of the WK and WKM. This outcome is consistent with earlier reports. (Kumar et al. 2014; Mubarak et al. 2016).

To determine the surface properties of WK and WKM, the nitrogen adsorption–desorption isotherm and Barrett–Joyner–Halenda (BJH) pore-size distribution methods were used. To achieve this, about 0.25 g of WK and WKM were degassed at 105 °C prior to BET run and the data obtained were analysed with Tristar II 3020 version 2 software and plotted on OriginPro 8.0. As displayed in Fig. 2, the N_2 isotherm is similar to type III, in that it has a high adsorption capacity but has broader pore-size distributions, narrower mesopores and wider micropores. The modest hysteresis loop at a relative pressure of $0.8 < P/P0 < 1$ in the N_2 adsorption–desorption isotherm indicates capillary condensation, suggesting the dominance of a mesoporous structure. The BET surface area of WKM from the N_2 adsorption analysis was 81.1184 $m^2 g^{-1}$, which is far greater than that of WK (0.7925 $m^2 g^{-1}$) (see Table 3). The large surface area of WKM was due the incorporation MWCNTs (modifier) to WK. Therefore, the increased surface area of the WKM provides a large storage area for RhB adsorption. A similar trend was noticed for the pore volume and pore diameter
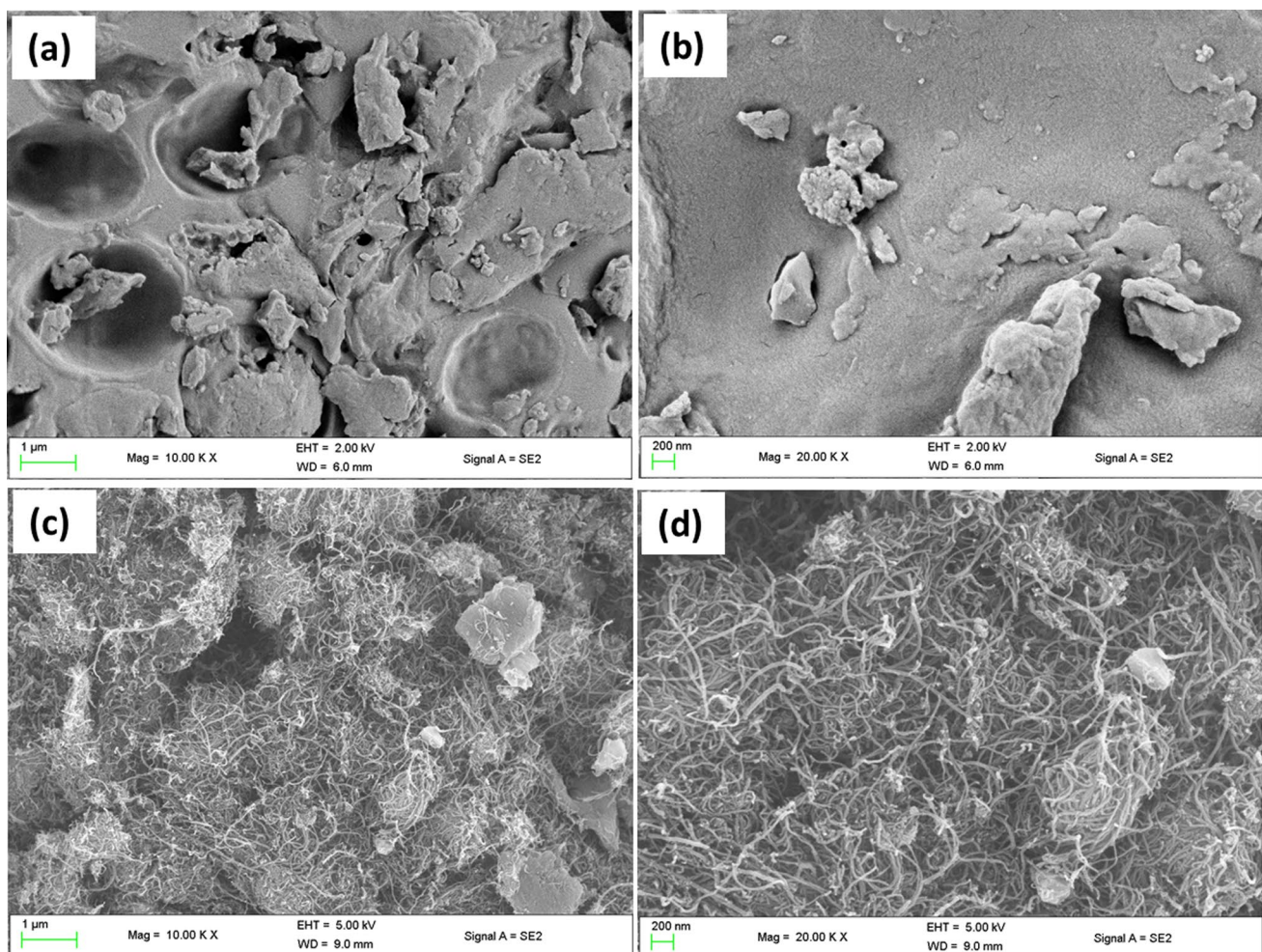

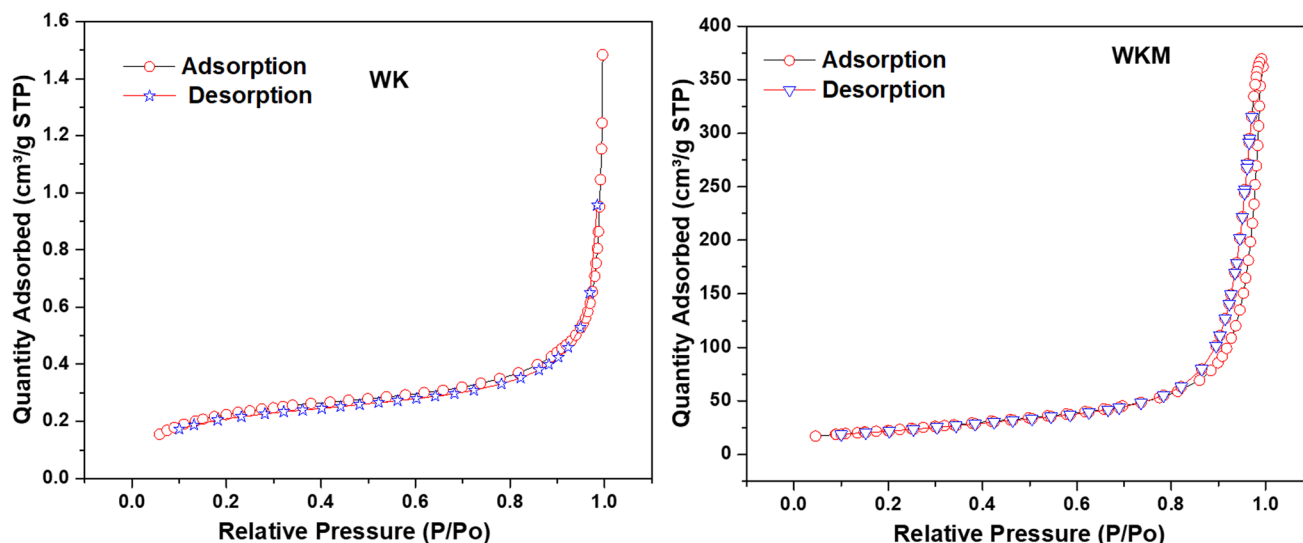**Fig. 1** FESEM micrographs of (**a**) WK, **b** WK–RhB, **c** WKM and **d** WKM–RhB

Fig. 2 N_2 adsorption/desorption isotherm of WK and WKM

Table 3 Surface characteristics of WK and WKM

Adsorbents	Surface area/$m^2\ g^{-1}$	Pore volume/$cm^3\ g^{-1}$	Pore diameter/nm	pH_{PZC}
WK	0.7925	0.001793	10.2268	6.68
WKM	81.1184	0.566600	27.9454	5.08

of both adsorbents. Hence, easy pore entrapment of RhB into the cavities of the nanocomposite could enhance the removal of RhB.

Thermogravimetric analysis

To establish the composition of the WKM and the behaviour of the nanocomposite at higher temperatures, the thermogram of the novel adsorbent (WKM) was acquired within the temperature range of 25–600 °C under a N_2 atmosphere. TG analysis of WKM revealed that the weight (4%) loss at temperatures below 100 °C was associated with the loss of moisture (see Fig. 3). Weight loss between 100 and 200 °C may be attributed to degradation of the crosslinker employed in the fabrication of the nanocomposite. The second pyrolytic stage may be attributed to the decomposition of the WK in the nanocomposite and the formation of volatile components (CO, CO_2, H_2 and CH_4) which accounted for almost 30% of the weight loss within the temperature range of 200–366 °C. The last stage (350–600 °C) accounted for 5% weight loss and can be attributed to partial oxidation of the MWCNTs. This result is in line with past work on the thermal behaviour of multi-walled carbon nanotube-based adsorbents (Sadegh et al. 2016; Zhan et al. 2018).

The chemical moieties of pristine and RhB-loaded adsorbents were investigated using FTIR (see Fig. 4). From the spectra, several peaks were noticed, indicating the
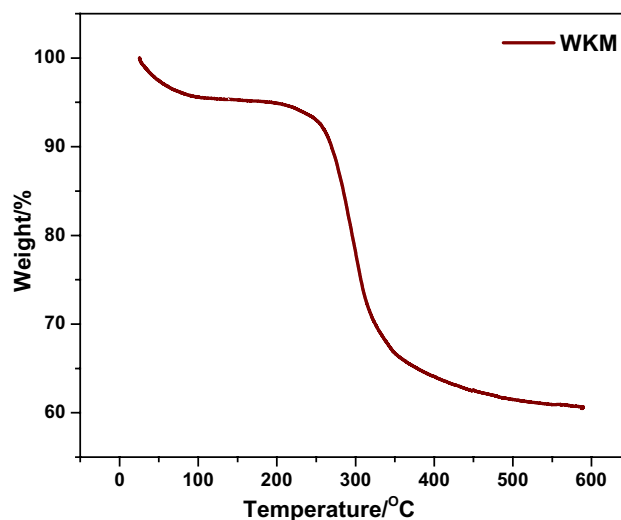

Fig. 3 The TGA thermograms of WKM

presence of different chemical moieties on the surfaces of the WK and WKM. Among these peaks include bands at 3312–3410 cm^{-1} and 2920–2933 cm^{-1} which were assigned to –OH and aliphatic C–H vibrational stretches, respectively (Rasana and Jayanarayanan 2022). Meanwhile, peaks at 1604–1648 cm^{-1}, 1382–1415 cm^{-1}, 991–1008 cm^{-1} and 751–784 cm^{-1} were attributed to –C=O, –C=O,–C–O–C–, –C-halogen, vibrational stretching (Alam et al. 2016; Omer
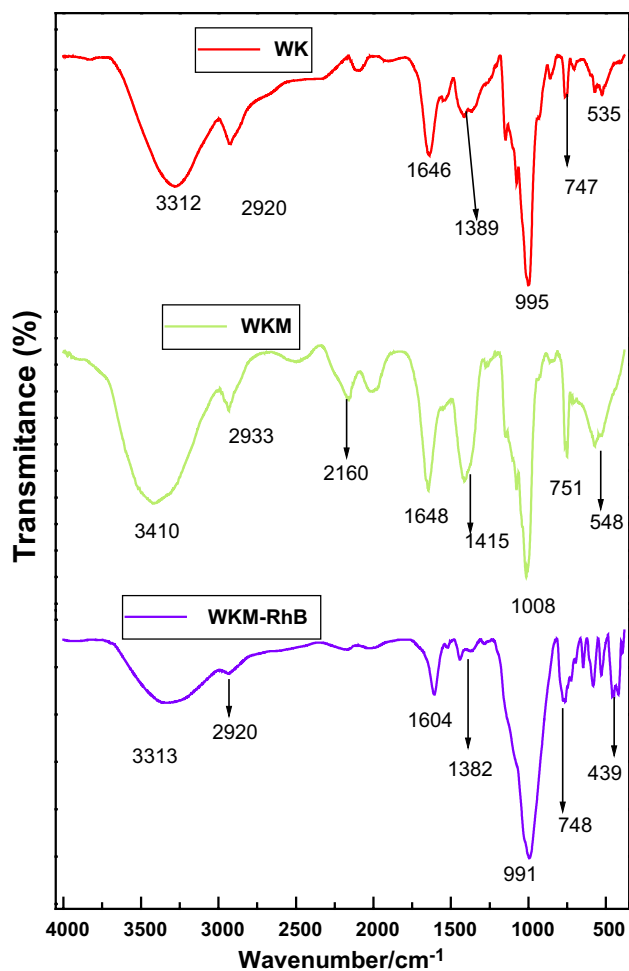
Fig. 4 The FTIR spectra of WK, WKM and WKM–RhB

Table 4 The observed FTIR spectral bands (cm^{-1}) and assignments

WK	WKM	WKM-Cr	Assignments
3312	3410	3313	υ(O–H, N–H)
2920	2933	2920	υ(C–H)
2019	2160		υ(C≡C)
1646	1648	1604	υ(C=O)
1415	1388	1382	υ(C=O)
995	1008	991	υ(C–O–C)
766	751	784	υ(C-halogen)
535	548	439	υ(C-halogen)

the other hand, diffraction peaks with 2θ values of 26.01° and 44.23°, 56.09° and 77.08° for WKM were obtained and indexed to the (002) and (100) (004) and (110) reflections of graphite from MWCNTs, respectively (ICDD No. 01-074-2379) (see Fig. 5). These peaks reflect the incorporation of the modifier (MWCNTs) to the nanocomposite. Hence, the nanocomposite was successfully synthesized.
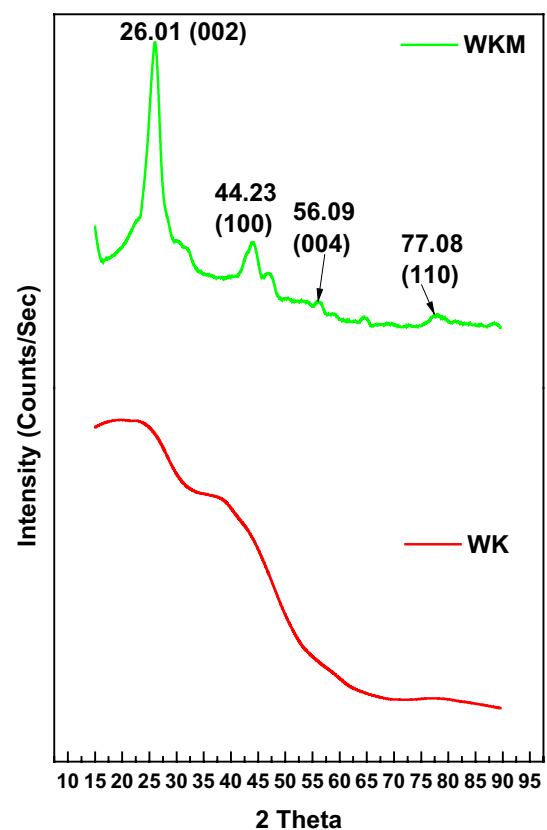
et al. 2018), respectively. Meanwhile, a comparison of spectra acquired for used and unused adsorbents revealed a shift in bands for spent adsorbents (WKM–RhB). Hence, a physicochemical interaction between the adsorbent (nanocomposite (WKM) and RhB molecule occurred. This corroborates with the deduction made on the FESEM analysis of WKM–RhB. Following the adsorption of RhB onto the nanocomposite, a shift in the band was observed as revealed by the spectra of WKM-Cr. This shows that the nanocomposite provided active sites for the uptake of the target adsorbate (RhB). In addition, the bands associated with WKM–RhB were shifted to lower frequencies as observed in the acquired spectrum (Table 4). This indicated the successful incorporation of the RhB to the surface of MWK.

The crystalline structure of the plant biomass (WK) and nanocomposite (WKM) was examined by means of powder XRD analysis. The samples were scanned from 15° to 90° using 2θ range with a step size of 0.02°, Cu Kα ($\lambda = 1.54050$ Å) radiation and a step rate of 0.454° s^{-1}. The biomass showed no resolute peaks in its diffractogram. On

Fig. 5 X-ray diffraction spectral for WK and WKM

Effect of pH

A cardinal factor of adsorption is the solution pH and this is because of its capacity to influence the surface chemistry of the adsorbent, ionization of adsorbate and impacts the mode of interaction (Batzias and Sidiras 2007; Gherbi et al. 2022). The surface charge of all adsorbents is known to be null, negative or positive. To validate the nature of charges on the adsorbent surface, point of zero charge (pH_{PZC}) experiment was performed. pH_{PZC} defines the pH for which the surface of the adsorbent will be zero. At pH values lower or higher than the pH_{PZC} of WKM and WK, the surfaces of these adsorbents (WKM and WK) will be positively charged and negatively charged, respectively. As shown in Fig. 6, the pH_{PZC} of WKM and WK were estimated as 5.08 and 6.68, respectively. The effect of pH on the uptake of RhB onto WKM and WK was assessed. The results revealed that the uptake of RhB by WKM and WK was favoured at lower pH values. The adsorbents were observed to be most effective at pH of 3 (see Fig. 6). As the pH increased from 4 to 10, a decrease in the capacity of WKM and WK to eliminate RhB from aqueous solution was observed (see Fig. 7). The high uptake of RhB by WKM and WK could be attributed to the monomeric nature of RhB at solution pH less than 3.7 (Zamouche and Hamdaoui 2012). This may enhance the pore entrapment of the cationic Rhodamine B (RhB^+) into the pore of WKM and WK in addition to hydrophobic interactions ($\pi–\pi$ stacking) of the dye molecules with the adsorbent surface.
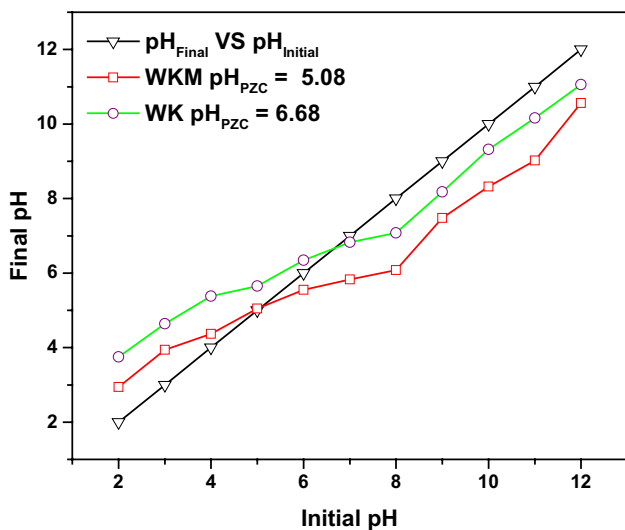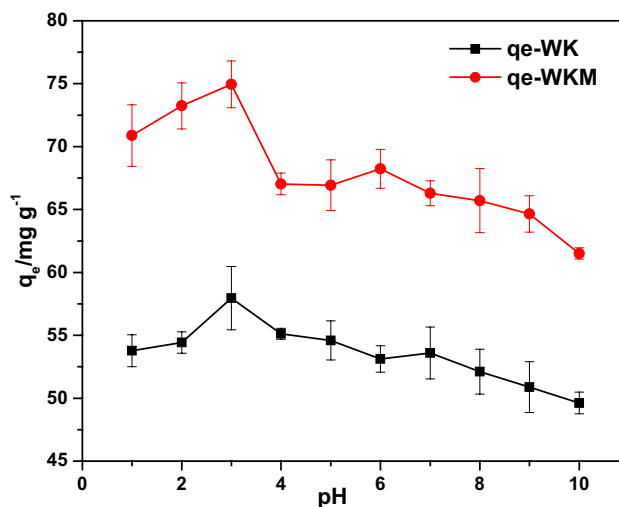

Fig. 7 Effect of initial solution pH on the uptake of RhB onto WKM and WK

Kinetics of adsorption

Essential information (removal rate and mechanism of adsorption) needed to develop an adsorption process is partly deduced from the kinetic analysis (Haro et al. 2021). The effect of contact time on the adsorption of RhB onto WKM and WK was assessed using a fixed concentration of 100 mg dm^{-3} (25 cm^3), agitation times ranging from 5 to 180 min and 0.05 g adsorbent dose at room temperature (see Fig. 8). An increase in the uptake capacity of WKM and WK with increased agitation time was observed in the adsorptive removal of RhB. This could be attributed to increase in site occupation by RhB with time.
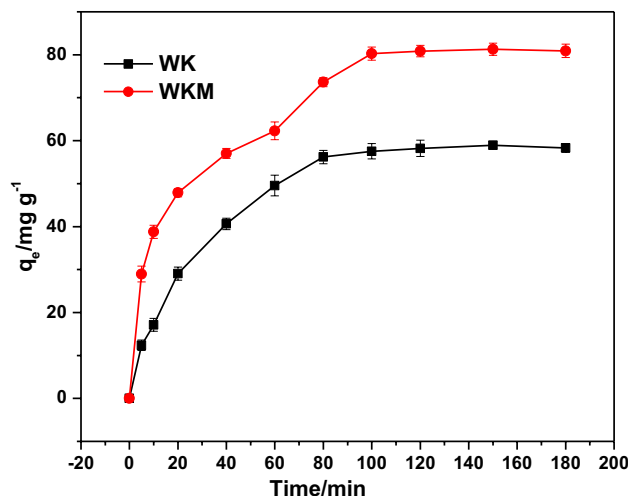

Fig. 6 pH_{PZC} plots of WK and WKM

Fig. 8 Effect of agitation time on the uptake of RhB by WK and WKM

Meanwhile, about 80.32 mg and 57.71 mg of RhB were sequestered per gram of WKM and WK after 100 min of contact. Thereafter, no substantial removal of RhB was observed for WKM and WK. As a result, 100 min was chosen as the best adsorption time. However, to ensure a complete adsorptive process, 180 min was used for further experiments. The kinetic modelling for the adsorptive removal of RhB by WKM and WK was evaluated using the intraparticle diffusion (ID), pseudo-first-order (PFO), Elovich and pseudo-second-order (PSO) model (see Fig. 9). Table 5 shows the parameters acquired from the kinetic model plots. For the adsorption of RhB onto WKM, it is clear that the procedure was closely expressed by the Elovich kinetic model based on the least value for the sum of squared residuals (SSR) and the residual standard error (RSE) when compared to other models. Meanwhile, this validates the report of most researchers on the uptake of RhB onto other adsorbents (Wang et al. 2017). This suggests a chemisorptive adsorption process. For the adsorption of RhB onto WK, PFO was noticed to best describe the acquired experimental data. Conventional kinetics models such as PFO and PSO lack the basics to offer information on the mechanism of diffusion of RhB into the pores of the WKM and WK. Values of intercepts extrapolated from the plots of $t^{1/2}$ versus q_{eq} indicate the inclusion of another rate-controlling step in the uptake of RhB onto WKM and WK (see Table 5). Meanwhile, owing to the fact that the plot did not go through the starting point suggests that intraparticle diffusion is not the only rate-determining mechanism but comprises some degree of boundary layer diffusion. This report is in good agreement with the result obtained for the uptake of RhB onto activated carbon composite (Hayeeye et al. 2017) and rice husk ash (Suc and Kim Chi 2017).

Table 5 Kinetics parameters for RhB adsorption onto WK and WKM

Model	Parameter	WK	WKM
Experimental	q_{exp}/mg g^{-1}	58.32	80.90
Pseudo-first-order	K_1/min^{-1}	0.0327	0.0515
	q_{eq}/mg g^{-1}	59.11	76.85
	SSR	23.54	491.9
	RSE	1.715	7.842
Pseudo-second order	K_2/g mg^{-1} min^{-1}	5.17 X 10^{-04}	7.98 X 10^{-04}
	q_{eq}/mg g^{-1}	70.81	86.79
	SSR	35.61	201.1
	RSE	2.110	5.013
	h	2.592	6.019
	$t_{0.5}$/min	27.32	14.43
Intraparticle diffusion	K_{id}/mg g^{-1} min$^{-0.5}$	5.324	7.415
	l/mg g^{-1}	8.448	24.38
	SSR	448.2	1259
	RSE	7.057	11.83
Elovich	α/mg g^{-1} min^{-1}	− 13.37	1.806
	β/g mg^{-1}	14.78	15.873
	SSR	86.35	90.66
	RES	3.285	3.366

Effect of dosage

The influence of adsorbent dosage was examined at pH 3 using 25 cm^3 of 100 mg dm^{-3} RhB solution and varying the WKM or WK dosage from 0.01 to 0.1 g. As displayed in Fig. 10, it was observed that as the adsorbent dosage was increased from 0.01 to 0.1 g, the percentage removal of RhB also increases up to 97.17% and 71.47% for WKM and WK,
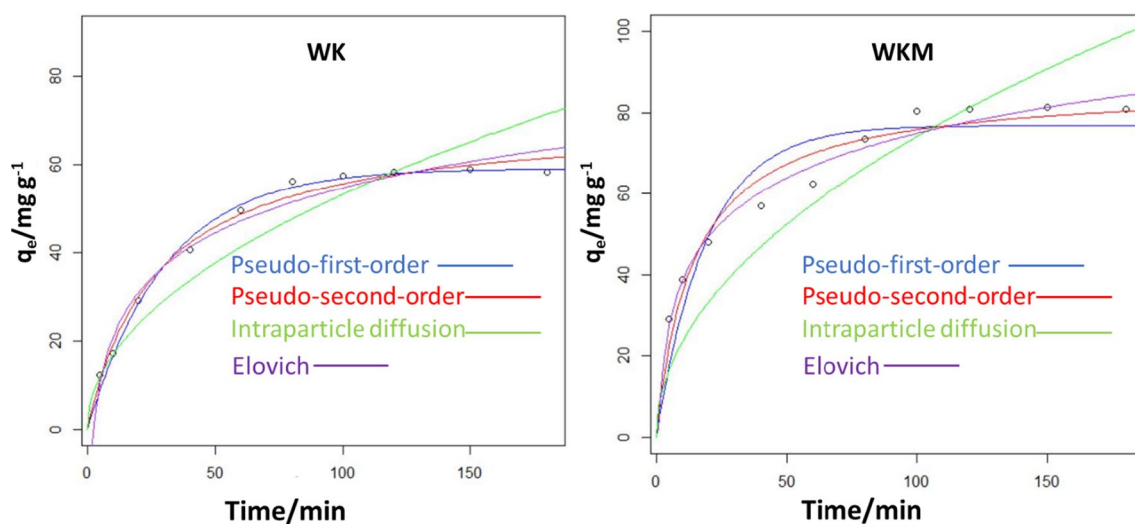

Figure. 9 Comparison of the various kinetics models fitted to the experimental data of RhB adsorption onto WK and WKM
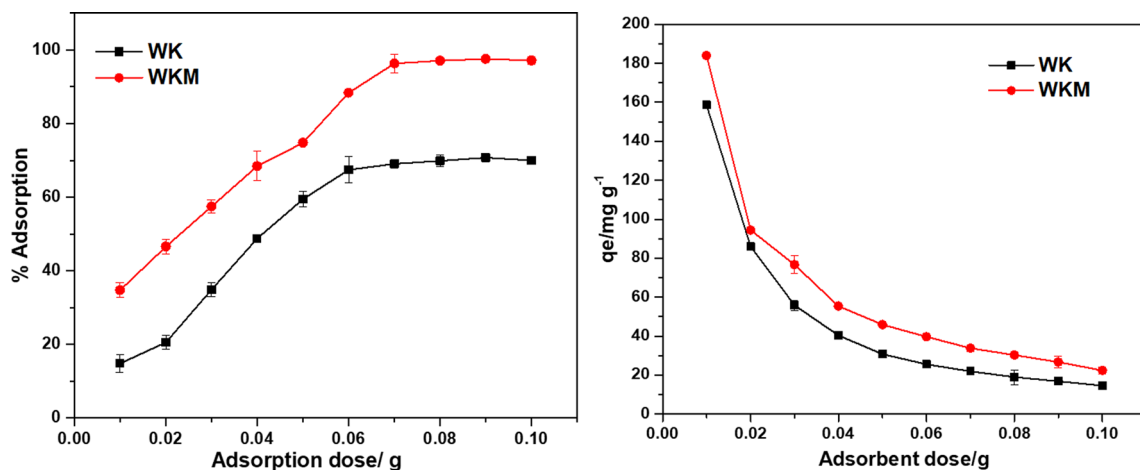
Figure. 10 Effect of dosage on the uptake efficiency (%) and the uptake capacity (q_{eq}) of RhB adsorption by WK and WKM

respectively. This could be ascribed to the availability of a sufficient number of active sites. It was further observed that at 0.5 g, more than 75% of RhB was eliminated from the aqueous solution. Hence, 0.05 g was accepted as the working adsorbent dose. On the other hand, the uptake capacity of WKM and WK was noticed to reduce from 192.34 to 23.17 mg g^{-1} and 91.19 to 19.37 mg g^{-1}, respectively. This phenomenon could be associated with the agglomeration of adsorbents that leads to binding site deprivation.

Adsorption isotherm

To validate the nature and affinity of sorbent-sorbate interaction and the characteristics of the adsorbent (WK and WKM) surface, isotherm modelling of the adsorptive removal of RhB by WK and WKM becomes exigent. To establish the aforementioned adsorptive characteristics,

the effect of initial RhB concentration experiment was evaluated and presented in Fig. 11. With the increase in the RhB concentration from 10 to 80 mg dm^{-3}, we observed a continuous increase in the adsorption capacity of WK and WKM. Above 80 mg dm^{-3}, equilibrium was noticed for the uptake of RhB onto WK at all temperatures investigated. A similar observation was made for WKM with the exception of higher solution temperatures (313 K and 318 K). Hence, 100 mg dm^{-3} was selected for further optimization process in order to guarantee maximum use of the active sites on WK and WKM. The increase in absorption capacity with concentration could be attributed to an increase in driving force caused by the greater concentration gradient, which improves RhB interaction with the active sites of WK and WKM. This result is in good agreement with the report on the adsorption of RhB onto carbon nanotube–cobalt ferrite nanocomposites (Oyetade
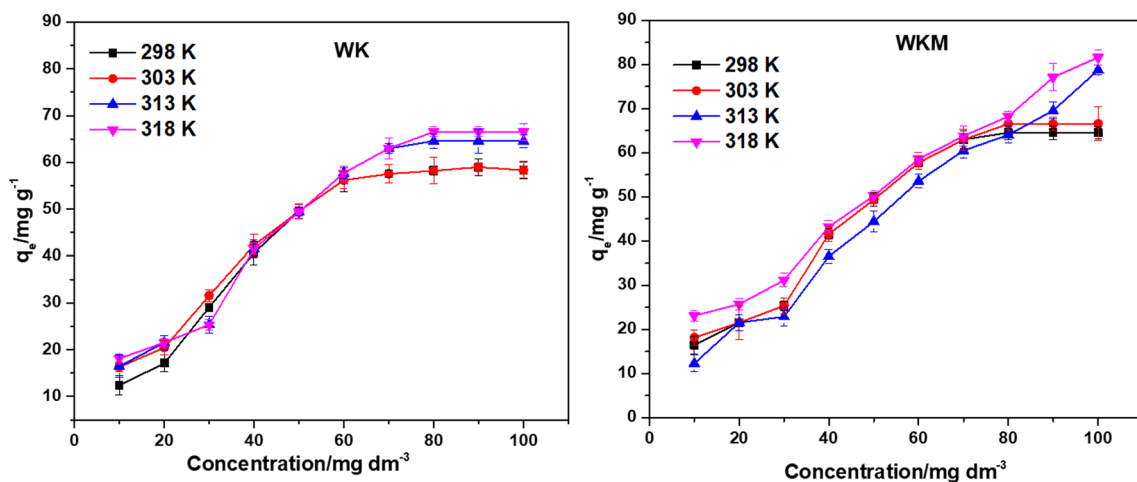

Fig. 11 Effect of initial RhB concentration and solution temperature on the adsorption capacity of WK and WKM for RhB

et al. 2015) and gelatin/activated carbon composite beads (Hayeeye et al. 2017).

The experimental data from the initial RhB concentration experiment were modelled using the Langmuir and Freundlich isotherms, as stated in the supplemental document. The estimated isotherm parameters obtained from the models are presented in Table 6. Isotherm models that best describe the uptake of RhB onto WKM and WK were selected because they had the least SSR and RSE. As observed, for the adsorption of RhB onto WKM and WK, the Freundlich model was noticed to best describe the experimental data acquired for both adsorbents. As a result, multilayer adsorption of RhB onto heterogeneous WKM and WK surfaces is suggested. (Herbert Freundlich 1907). The deduction from the Freundlich model (heterogeneous uptake of RhB onto WKM and WK) was confirmed by FESEM images of the WKM and WK, which revealed an uneven surface morphology with sheet-like particles of diverse sizes and shapes. The affinity between the RhB and the novel adsorbent (WKM and WK) can be deduced from the Freundlich n value. Meanwhile, n values between 1 and 10 indicate a favourable adsorption process (Chen et al. 1999; Fo and Odebunmi 2010). Hence, the uptake of RhB onto WKM and WK was favourable. On the other hand, the maximum uptake capacity as deduced from Langmuir adsorption Isotherm was 67.58 mg g^{-1} and 67.82 mg g^{-1} for WKM and WK, respectively. These values showed the superior potential of WKM and WK when compared with the monolayer adsorption capacity of other adsorbents (see Table 8). Hence, WKM and WK have demonstrated the potential for environmental remediation of RhB from contaminated water.

Adsorption thermodynamics

We also computed thermodynamic parameters (i.e. standard free energy change ($\Delta G°$), enthalpy change ($\Delta H°$) and entropy change ($\Delta S°$)) to analyse critical information regarding the adsorption process's exothermic/endothermic nature, degree of unpredictability and feasibility (see Table 7). These parameters were estimated using equations

S3 and S4 as described in the supplementary information. The thermodynamic analysis for the adsorption of RhB onto WKM and WK was noticed to be significant at elevated solution temperature (see Fig. 11). This could be attributed to the enhanced kinetic energy of the RhB molecules, leading to frequent interaction with the adsorption site that could result to an effective collision. It could also be due to the enlargement of sorbent pores resulting to increase RhB removal (Al-Rashed and Al-Gaid 2012). This result is consistent with the report on the adsorption of RhB onto kaolinite (Khan et al. 2012) and agricultural by-products (Gad and El-Sayed 2009). It is apparent that the uptake of RhB molecule onto WKM and WK was an endothermic process. Table 7 presents the thermodynamic parameters estimated for the adsorption of RhB onto WKM and WK. Negative $\Delta G°$ values were estimated at all temperatures for the adsorption of RhB onto WKM and WK. This indicates the potential of WKM and WK to decontaminate RhB-loaded wastewater. This is consistent with the report on the uptake of RhB onto kaolinite (Khan et al. 2012). Meanwhile, positive $\Delta S°$ values of 352.5 J K^{-1} mol^{-1} and 101.1 J K^{-1} mol^{-1} suggested a rise in randomness at the RhB-WKM and RhB-WK interfaces, respectively, during the adsorption process. It has been reported that $\Delta H°$ values higher than 40 kJ/mol and $\Delta H°$ values less than 40 kJ/mol indicate chemisorption and

Table 7 Thermodynamic parameters for the uptake of RhB onto WK and WKM

Adsorbents	T/K	$\Delta G°$/kJ mol^{-1}	ΔH/kJ mol^{-1}	ΔS/J K^{-1} mol^{-1}
WK	298	−21.0881	8.926	101.1
	303	−20.1736		
	308	−20.7003		
	318	−21.4311		
WKM	298	−20.8868		
	303	−21.679	84.11	352.5
	308	−23.8022		
	318	−29.2042		

Table 6 Isotherm parameters for RhB uptake onto WK and WKM

| Adsorbent	Isotherm	Parameters		Temperature		
			295 K	303 K	310 K	318 K
WK	Freundlich	K_F	0.5850351	0.3515369	0.4667416	0.3462435
		n	1.1150996	0.9858996	1.0408117	0.9643428
		SSR	39.48924	56.77381	46.5622	67.9003
		RSE	2.222	2.664	2.413	2.913
WKM	Freundlich	K_F	2.3326780	6.896058	13.052275	37.679735
		n	0.8107321	1.094605	1.378699	3.197042
		SSR	2361.776	2063.664	2186.4424	3281.6985
		RSE	17.18	16.06	16.53	20.25
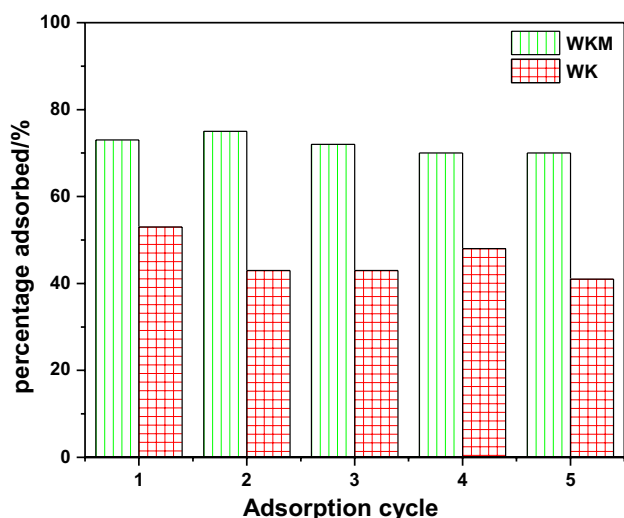
Fig. 12 The RhB removal efficiency of WK and WKM after different cycles

physisorption adsorptive process, respectively. Hence, the adsorptive removal of RhB by WKM and WK was dominated by chemisorption and physisorption, respectively.

This further corroborates with the SEM results and the isotherm analysis obtained for WKM (see Table 6).

Desorption and reusability

In wastewater treatment practice, economically viable adsorbents are materials with sustainable uptake potential that possesses excellent regeneration and reuse characteristics (Dai et al. 2019; Dutta et al. 2019). Besides, the application of non-toxic and inexpensive eluting solvents in the regeneration process was observed. The sustainability of a high uptake potential after several cycles is also a vital criterion in assessing the value of any adsorbent. The desorption of RhB from the surface of the adsorbent has been investigated using different concentrations of HNO_3, HCl and NaOH solutions (Suc and Kim Chi 2017). Hence, the choice of NaOH as eluent was selected. The preliminary desorption showed about 90% of RhB desorbed using 0.1 M NaOH, this also suggests an anion exchange mechanism during the adsorption and desorption processes. Figure 12 shows the reusability of the WKM and WK for RhB adsorption after five adsorption–desorption cycles. We
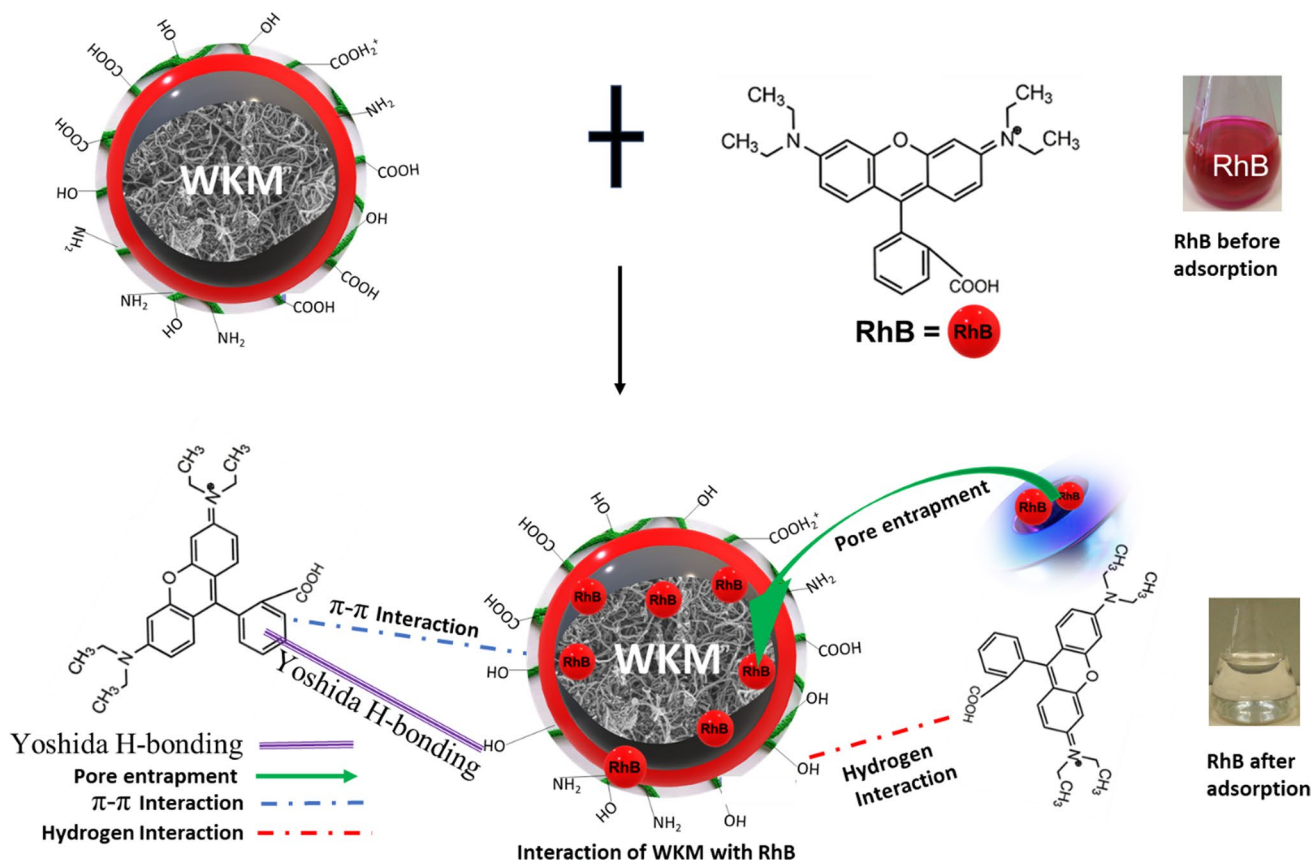

Figure. 13 Mechanisms of interaction that could exist between WKM and RhB

observed a modest decrease in the adsorption efficiency of RhB from 85.60 to 80.73% and 54.78 to 41.43% for WKM and WK from the initial uptake to the fifth cycle of reuse, respectively. Hence, WKM has demonstrated a superior capacity for environmental radiation practices.

Mechanism of adsorption

In order to establish the mechanism responsible for the adsorption of RhB on WKM, the physicochemical properties of spent and pristine of WKM were assessed by making use of SEM and FTIR spectroscopic techniques. Besides the spectroscopic techniques, adsorption parameter, such as solution pH, was also considered for the elucidation of mechanism responsible for the uptake of RhB onto WKM. The influence of solution pH on the speciation of RhB gives insight into chemistry of RhB during uptake. RhB is in the zwitterionic state (pH > pKa with pKa = 3.7). The zwitterionic form of RhB in water may promote aggregation of RhB to create a bigger molecular form (dimer) and become impossible to enter the pore of WKM at pH values greater than 3.7. The favourable electrostatic interactions between the carboxyl and xanthene groups of the monomers cause the zwitterionic form to aggregate more. Hence, favourable removal of RhB in the lower pH can be attributed to pore entrapment. This could be responsible for the

Table 8 Comparison of the Langmuir maximum adsorption capacities for RhB onto AMC, WK and WKM with those of other sorbents

Adsorbents	RhB	Reference
Ag@AgBr/SBA-15	18.52	Hu et al. (2015)
Sugarcane dust	4.26	Khattri and Singh (1999)
Argemone Mexicana	6.40	Khamparia and Jaspal (2016)
MWCNT	3.530	Kumar et al. (2014)
Orange peel	3.230	Namasivayam et al. (1996)
Magnetic bentonite	62.15	Wan et al. (2015)
Fe_3O_4/MWCNT	11.44	Kerkez and Bayazit (2014)
MWCNT-Fe_3O_4 (75%)	35.91	Oyetade et al. (2015)
Acacia nilotica	22.40	Santhi et al. (2014)
Cedar Cone	4.550	Zamouche and Hamdaoui (2012)
Kaolinite	46.08	Khan et al. (2012)
Fly ash	10.00	Chang et al. (2009a)
Jute stick powder	87.70	Panda et al. (2009)
Luffa cylindrical fibre	9.900	Altınışık et al. (2010)
Activated carbon prepared from tamarind fruit shells	4.570	Vasu (2008)
WK	67.82	This study
KWM	87.58	This study

swelling characteristics observed on using SEM. Meanwhile, FTIR revealed shift in –OH and –C=C– peaks, this suggests the inclusion of intermolecular hydrogen bonding or Yoshida H-bonding and π–π interaction, respectively. This may be resposible for the superior capacity of WKM (see Table 8). Hence, a collection of reaction path was responsible for the adsorption of RhB onto WKM (see Fig. 13).

Conclusions

This study demonstrated the fabrication of nanocomposite using *Buchholzia coriacea* pod and MWCNTs. The adsorbents (WK and WKM) were examined as value-added adsorbents for RhB adsorption, and it was found that the uptake capacity of WK and WKM during RhB removal was higher than the potential of most adsorbents reported in the literature. Moreover, optimal conditions such as 100 min, solution pH 3.0 and adsorbent dose of 0.05 g were determined for the uptake of RhB onto WK and WKM. Meanwhile, maximum monolayer capacity (q_{max}) of 67.82 mg g^{-1} and 87.58 mg g^{-1} was determined for WK and WKM. The kinetics for the uptake of RhB onto WK and WKM was best described by pseudo-first-order and Elovich, respectively. On the other hand, the Freundlich isotherm models were noticed to describe the equilibrium data acquired for the uptake of RhB onto WK and WKM. The excellent performance of WK and WKM presents these materials as promising adsorbents for the sequestration of dye from textile wastewater.

Declarations

References

Abdullah TA, Juzsakova T, Hafad SA, Rasheed RT, Al-Jammal N, Mallah MA, Aldulaimi M (2022) Functionalized multi-walled carbon nanotubes for oil spill cleanup from water. Clean Technol Environ Policy 24(2):519–541

Adewoye T, Ogunleye O, Abdulkareem A, Salawudeen T, Tijani J (2021) Optimization of the adsorption of total organic carbon from produced water using functionalized multi-walled carbon nanotubes. Heliyon 7(1)

Aksu Z, Karabayır G (2008) Comparison of biosorption properties of different kinds of fungi for the removal of Gryfalan Black RL metal-complex dye. Bioresour Technol 99(16):7730–7741

Al-Rashed SM, Al-Gaid AA (2012) Kinetic and thermodynamic studies on the adsorption behavior of Rhodamine B dye on Duolite C-20 resin. J Saudi Chem Soc 16(2):209–215

Alam RS, Moradi M, Nikmanesh H (2016) Influence of multi-walled carbon nanotubes (MWCNTs) volume percentage on the magnetic and microwave absorbing properties of $BaMg_{0.5}Co_{0.5}TiFe_{10}O_{19}$/MWCNTs nanocomposites. Mater Res Bull 73:261–267

Altınışık A, Gür E, Seki Y (2010) A natural sorbent, Luffa cylindrica for the removal of a model basic dye. J Hazard Mater 179(1):658–664

Balistrieri L, Murray JW (1981) The surface chemistry of goethite (alpha FeOOH) in major ion seawater. Am J Sci 281(6):788–806

Batzias F, Sidiras D (2007) Simulation of dye adsorption by beech sawdust as affected by pH. J Hazard Mater 141(3):668–679

Belachew N, Hinsene H (2020) Preparation of cationic surfactant-modified kaolin for enhanced adsorption of hexavalent chromium from aqueous solution. Appl Water Sci 10(1):38

Chang S-H, Wang K-S, Li H-C, Wey M-Y, Chou J-D (2009a) Enhancement of Rhodamine B removal by low-cost fly ash sorption with Fenton pre-oxidation. J Hazard Mater 172(2):1131–1136

Chang S-H, Wang K-S, Li H-C, Wey M-Y, Chou J-D (2009b) Enhancement of Rhodamine B removal by low-cost fly ash sorption with Fenton pre-oxidation. J Hazard Mater 172(2–3):1131–1136

Chen Z, Xing B, McGill W (1999) A unified sorption variable for environmental applications of the Freundlich equation (0047–2425). Retrieved from

Dai Y, Zhang N, Xing C, Cui Q, Sun Q (2019) The adsorption, regeneration and engineering applications of biochar for removal organic pollutants: a review. Chemosphere 223:12–27

Das SK, Bhowal J, Das AR, Guha AK (2006) Adsorption behavior of rhodamine B on rhizopus o ryzae biomass. Langmuir 22(17):7265–7272

Du L, Wu J, Hu C (2012) Electrochemical oxidation of rhodamine B on RuO_2–PdO–TiO_2/Ti electrode. Electrochim Acta 68:69–73

Dutta T, Kim T, Vellingiri K, Tsang DC, Shon J, Kim K-H, Kumar S (2019) Recycling and regeneration of carbonaceous and porous materials through thermal or solvent treatment. Chem Eng J 364:514–529

Fo O, Odebunmi E (2010) Freundlich and Langmuir isotherms parameters for adsorption of methylene blue by activated carbon derived from agrowastes. Adv Nat Appl Sci 4:281–288

Freundlich H (1906) Over the adsorption in solution. J Phys Chem 57(385):e470

Freundlich H (1907) Über die adsorption in lösungen. Z Phys Chem 57(1):385–470

Gad HMH, El-Sayed AA (2009) Activated carbon from agricultural by-products for the removal of Rhodamine-B from aqueous solution. J Hazard Mater 168(2–3):1070–1081. https://doi.org/10.1016/j.jhazmat.2009.02.155

Gherbi B, Laouini SE, Meneceur S, Bouafia A, Hemmami H, Tedjani ML, Menaa F (2022) Effect of pH value on the bandgap energy and particles size for biosynthesis of ZnO nanoparticles: efficiency for photocatalytic adsorption of methyl orange. Sustainability 14(18):11300

Gupta VK, Kumar R, Nayak A, Saleh TA, Barakat MA (2013) Adsorptive removal of dyes from aqueous solution onto carbon nanotubes: a review. Adv Colloid Interface Sci 193–194:24–34. https://doi.org/10.1016/j.cis.2013.03.003

Gupta VK, Mohan D, Sharma S, Sharma M (2000) Removal of basic dyes (rhodamine B and methylene blue) from aqueous solutions using bagasse fly ash. Sep Sci Technol 35(13):2097–2113

Gupta VK, Saleh TA (2013) Sorption of pollutants by porous carbon, carbon nanotubes and fullerene-an overview. Environ Sci Pollut Res 20(5):2828–2843

Haro NK, Dávila IVJ, Nunes KGP, de Franco MAE, Marcilio NR, Féris LA (2021) Kinetic, equilibrium and thermodynamic studies of the adsorption of paracetamol in activated carbon in batch model and fixed-bed column. Appl Water Sci 11:1–9

Hayeeye F, Sattar M, Chinpa W, Sirichote O (2017) Kinetics and thermodynamics of Rhodamine B adsorption by gelatin/activated carbon composite beads. Colloids Surf A 513:259–266. https://doi.org/10.1016/j.colsurfa.2016.10.052

Hoang AT, Nižetić S, Cheng CK, Luque R, Thomas S, Banh TL, Nguyen XP (2022) Heavy metal removal by biomass-derived carbon nanotubes as a greener environmental remediation: a comprehensive review. Chemosphere 287:131959

Hou M-F, Ma C-X, Zhang W-D, Tang X-Y, Fan Y-N, Wan H-F (2011) Removal of rhodamine B using iron-pillared bentonite. J Hazard Mater 186(2–3):1118–1123

Hu L, Yuan H, Zou L, Chen F, Hu X (2015) Adsorption and visible light-driven photocatalytic degradation of Rhodamine B in aqueous solutions by Ag@ AgBr/SBA-15. Appl Surf Sci 355:706–715

Jain R, Mathur M, Sikarwar S, Mittal A (2007) Removal of the hazardous dye rhodamine B through photocatalytic and adsorption treatments. J Environ Manag 85(4):956–964

Kadirvelu K, Karthika C, Vennilamani N, Pattabhi S (2005) Activated carbon from industrial solid waste as an adsorbent for the removal of Rhodamine-B from aqueous solution: kinetic and equilibrium studies. Chemosphere 60(8):1009–1017

Kerkez Ö, Bayazit ŞS (2014) Magnetite decorated multi-walled carbon nanotubes for removal of toxic dyes from aqueous solutions. J Nanopart Res 16(6):2431

Khalatbary M, Sayadi MH, Hajiani M, Nowrouzi M (2022) Adsorption studies on the removal of malachite green by γ-Fe_2O_3/MWCNTs/cellulose as an eco-friendly nanoadsorbent. Biomass Convers Biorefinery 1–19

Khamparia S, Jaspal D (2016) Investigation of adsorption of Rhodamine B onto a natural adsorbent *Argemone mexicana*. J Environ Manag 183:786–793

Khan TA, Dahiya S, Ali I (2012) Use of kaolinite as adsorbent: equilibrium, dynamics and thermodynamic studies on the adsorption of Rhodamine B from aqueous solution. Appl Clay Sci 69:58–66

Khattri S, Singh M (1999) Colour removal from dye wastewater using sugar cane dust as an adsorbent. Adsorpt Sci Technol 17(4):269–282

Kumar S, Bhanjana G, Jangra K, Dilbaghi N, Umar A (2014) Utilization of carbon nanotubes for the removal of Rhodamine B dye from aqueous solutions. J Nanosci Nanotechnol 14(6):4331–4336

Langmuir I (1918) The adsorption of gases on plane surface of glass, mica and platinum. J Am Chem Soc 40(9):1361–1403. https://doi.org/10.1021/ja02242a004

Lim CC, Shuit SH, Ng QH, Rahim SKEA, Hoo PY, Yeoh WM, Goh SW (2023) Sulfonated magnetic multi-walled carbon nanotubes with enhanced bonding stability, high adsorption performance,

and reusability for water remediation. Environ Sci Pollut Res 30(14):40242–40259

Liu Y, Chen M, Yongmei H (2013) Study on the adsorption of Cu (II) by EDTA functionalized Fe_3O_4 magnetic nano-particles. Chem Eng J 218:46–54

Marking LL (1969) Toxicity of rhodamine B and fluorescein sodium to fish and their compatibility with antimycin A. Progress Fish-Cult 31(3):139–142

Mittal H, Mishra SB (2014) Gum ghatti and Fe_3O_4 magnetic nanoparticles based nanocomposites for the effective adsorption of rhodamine B. Carbohyd Polym 101:1255–1264

Mubarak NM, Sahu JN, Abdullah EC, Jayakumar NS (2016) Rapid adsorption of toxic Pb (II) ions from aqueous solution using multiwall carbon nanotubes synthesized by microwave chemical vapor deposition technique. J Environ Sci

Namasivayam C, Muniasamy N, Gayatri K, Rani M, Ranganathan K (1996) Removal of dyes from aqueous solutions by cellulosic waste orange peel. Bioresour Technol 57(1):37–43

Ofomaja A, Naidoo E, Modise S (2009) Removal of copper (II) from aqueous solution by pine and base modified pine cone powder as biosorbent. J Hazard Mater 168(2):909–917

Omer A, Khalifa R, Hu Z, Zhang H, Liu C, Ouyang X-k (2018) Fabrication of tetraethylenepentamine functionalized alginate beads for adsorptive removal of Cr (VI) from aqueous solutions. Int J Biol Macromol

Omorogie MO, Babalola JO, Unuabonah EI, Gong JR (2016) Clean technology approach for the competitive binding of toxic metal ions onto MnO_2 nano-bioextractant. Clean Technol Environ Policy 18(1):171–184

Oyetade OA, Nyamori VO, Martincigh BS, Jonnalagadda SB (2015) Effectiveness of carbon nanotube–cobalt ferrite nanocomposites for the adsorption of rhodamine B from aqueous solutions. RSC Adv 5(29):22724–22739

Panda GC, Das SK, Guha AK (2009) Jute stick powder as a potential biomass for the removal of congo red and rhodamine B from their aqueous solution. J Hazard Mater 164(1):374–379

Rasana N, Jayanarayanan K (2022) Nano, micro and multiscale filler-reinforced functionalized polypropylene composites: FTIR characterization and mechanical study. Polyolefins J 9(1):33–43

Sadegh H, Zare K, Maazinejad B, Shahryari-ghoshekandi R, Tyagi I, Agarwal S, Gupta VK (2016) Synthesis of MWCNT-COOH-Cysteamine composite and its application for dye removal. J Mol Liq 215:221–228

Santhi T, Prasad AL, Manonmani S (2014) A comparative study of microwave and chemically treated *Acacia nilotica* leaf as an eco friendly adsorbent for the removal of rhodamine B dye from aqueous solution. Arab J Chem 7(4):494–503

Sarwar T, Khan S (2022) Textile industry: pollution health risks and toxicity. In: Textile wastewater treatment: sustainable bio-nano materials and macromolecules, vol 1. Springer, pp 1–28

Selvam PP, Preethi S, Basakaralingam P, Thinakaran N, Sivasamy A, Sivanesan S (2008) Removal of rhodamine B from aqueous solution by adsorption onto sodium montmorillonite. J Hazard Mater 155(1–2):39–44

Sevim AM, Hojiyev R, Gül A, Çelik MS (2011) An investigation of the kinetics and thermodynamics of the adsorption of a cationic cobalt porphyrazine onto sepiolite. Dyes Pigment 88(1):25–38. https://doi.org/10.1016/j.dyepig.2010.04.011

Skjolding LM, Dyhr K, Köppl C, McKnight U, Bauer-Gottwein P, Mayer P, Baun A (2021) Assessing the aquatic toxicity and environmental safety of tracer compounds Rhodamine B and Rhodamine WT. Water Res 197:117109

Suc NV, Kim Chi D (2017) Removal of rhodamine B from aqueous solution via adsorption onto microwave-activated rice husk ash. J Dispers Sci Technol 38(2):216–222. https://doi.org/10.1080/01932691.2016.1155153

Ukaogo PO, Ewuzie U, Onwuka CV (2020) Environmental pollution: causes, effects, and the remedies. In: Microorganisms for sustainable environment and health. Elsevier, pp 419–429

Vasu AE (2008) Studies on the removal of Rhodamine B and malachite green from aqueous solutions by activated carbon. J Chem 5(4):844–852

Vyawahare S, Pradhan SK, Gupta S (2014) Removal of heavy metal ions from industrial waste water using metallic nanoparticles as adsorbents. Adv Sci Lett 20(7–8):1311–1315

Wan D, Li W, Wang G, Chen K, Lu L, Hu Q (2015) Adsorption and heterogeneous degradation of rhodamine B on the surface of magnetic bentonite material. Appl Surf Sci 349:988–996

Wang G, Qi J, Wang S, Wei Z, Li S, Cui J, Wei W (2017) Surface-bound humic acid increased rhodamine B adsorption on nanosized hydroxyapatite. J Dispers Sci Technol 38(5):632–641. https://doi.org/10.1080/01932691.2016.1185729

Wu J, Gao C (2009) Click chemistry approach to rhodamine B-capped polyrotaxanes and their unique fluorescence properties. Macromol Chem Phys 210(20):1697–1708

Zamouche M, Hamdaoui O (2012) Sorption of Rhodamine B by cedar cone: effect of pH and ionic strength. Energy Procedia 18:1228–1239

Zhan Y, Wan X, He S, He Y (2018) Sulfonated poly (arylene ether nitrile)/polypyrrole core/shell nanofibrous mat: an efficient absorbent for the removal of hexavalent chromium from aqueous solution. J Chem Technol Biotechnol 93(5):1432–1442

Zhao X, Zhu Y (2006) Synergetic degradation of rhodamine B at a porous $ZnWO_4$ film electrode by combined electro-oxidation and photocatalysis. Environ Sci Technol 40(10):3367–3372

Zubrik A, Matik M, Hredzák S, Lovás M, Danková Z, Kováčová M, Briančin J (2017) Preparation of chemically activated carbon from waste biomass by single-stage and two-stage pyrolysis. J Clean Prod 143:643–653